INTERNATIONAL JOURNAL FOR NUMERICAL AND ANALYTICAL METHODS IN GEOMECHANICS, VOL. 21, 1–13 (1997)

APPLICATION OF A SPLITTING FRACTURE MODEL TO THE SIMULATION OF ROCK INDENTATION SUBSURFACE FRACTURES

X. C. TAN, P.-A. LINDQVIST AND S. Q. KOU

Department of Civil and Mining Engineering, Luleå University of Technology, S-97187 Sweden

SUMMARY

A two-dimensional fracture model based on micro-fracture mechanics is applied to the Hertzian indentation stress field to simulate subsurface fractures in an axi-symmetrical plane. The simulation of fracture development reveals quantitatively the effects of loading force, mechanical properties of the rocks, and original micro cracks on the formation of subsurface fractures. The distribution patterns of the subsurface fractures are determined by the magnitudes and trajectories of the indentation stresses. Lateral confinement prohibits the fracture development. Simulations of the subsurface fractures in granite and marble are in good agreement with the indentation experiments.

KEY WORDS: rock; indentation; fracture modelling; splitting fracture; damage

INTRODUCTION

Rock indentation is a fundamental process for rock excavation and fragmentation using mechanical methods. A sound understanding of rock fragmentation mechanisms and quantitative evaluation of parametric influences, such as rock properties and tool characteristics, is of great help in designing rock tools and equipment and in evaluation of damages to the rock body. The study of rock indentation is therefore important from both practical and theoretical points of view.

Researchers have carried out rock indentation tests extensively since the early 70s.[1–7] Rocks from sedimentary to igneous types have been tested under quasi static and dynamic loading conditions. It has been observed that during indentation the rock underneath the indenter undergoes crushing, fracturing and chipping. Analysis of rock indentation has mostly concerned tool penetration and rock failure at the surface, mainly because rock is not transparent and it is difficult to trace the propagation of rock fracture and fragmentation within the rock.

Rock failure by indentation has been evaluated using some conventional strength criteria. Typical results can be found in the work done by Korbin,[13] Sikarskie and Altiero[7] and others.[8–12] It has been found that the rock indentation strength, which was defined as the average contact pressure at peak load, was a few times larger than the uniaxial compressive strength of the rock, depending on the tool geometry, tool size and confining condition.[4,12] Rock chipping was assumed to take place along an inclined line to the surface by shear failure. Through a force balance and strength analysis with respect to the assumed failure line the relation of indenter penetration and rock chipping to the indentation load was obtained.[7] This described the rock fragmentation process, but it did not indicate the rock damage and fractures that developed

CCC 0363–9061/97/010001–13

Received 21 February 1996
Revised 26 April 1996

within the rock. The work discussed above mainly concerned wedge type tools and the results are not readily applicable to other indenter shapes.

Fracture mechanics has been applied to the study of rock fragmentation by cutting.[13,14] In the conception of fracture mechanics, rock fragmentation and damage result from the development and interaction of fractures. For example, the rock cutting process was simulated by using the fracture mechanics criterion coupled to a numerical method,[14] which described the development of the fractures and predicted the detailed process of fragmentation by a drag bit. By using fracture mechanics it is possible to consider the physical process of material disintegration and to study closely the mechanisms of major fractures and fragments. This will lead to a further understanding and quantification of the rock fragmentation process.

Proper use of fracture models and determination of fracture parameters are important. The fundamental fracture criteria, for instance, the maximum stress criteria for the mode I to III cracks, can easily be applied to predict the initiation of the cracks in a simple stress field. However they cannot predict the length and direction of crack propagation. For these purposes, numerical methods, which require often complicated calculations of stresses and fracture parameters, have to be used.

The indentation stress field is not uniform. The stresses are extremely large close to the loading point and decrease rapidly with increasing distance from the loading point. For the study of rock engineering problems it is highly desirable that a relatively simple and concise model be developed to provide both physical understanding and prediction of the process.

Fracture of brittle rock in compression is widely observed in rock engineering, for instance, hole breakout and pillar instability, and has been studied by a number of researchers.[15–18] It is quite clear that the deformation of brittle rocks in compression is accompained by the initiation and development of a multitude of pre-existing micro cracks from a certain level of load. After reaching a peak load, a shear band is formed gradually due to bridging of these fractures and finally the rock loses its capability to sustain any load. The fractures, which are initiated by shear, develop first along curved paths and then in the direction of compression. This type of fracture is called splitting fracture and could not be accounted for directly by any of the existing fracture criteria (model I to mode III). Models to describe brittle fracture phenomena in compression have been developed, most of them employing the sliding cracks in two dimensions. However, not all of them offer realistic deformation behaviour. The constitutive model developed by Li and Nordlund[16] incorporated the splitting fracture mechanism and represented the whole process of deformation and failure very well. The model combined four deformation components: (i) the response of the rock matrix; (ii) closure of the open cracks; (iii) the component due to fracture; and (iv) the component due to the shear failure. The treatment of splitting fractures and prediction of the steady growth of the splitting fractures under axial compression and lateral confinement were carried out in a simplified manner.

In this paper, propagation of the rock subsurface cracks caused by a hemispherical indenter is simulated using this splitting fracture model. The effects of influencing factors such as loading force, indenter shape, and rock properties on crack propagation are examined. The features and validity of the model are also discussed.

MODELLING OF SUBSURFACE ROCK INDENTATION FRACTURES

Rock indentation experimental results

Lindqvist *et al.*[19] conducted a series of rock indentation tests and observed the cracks on a large number of the indented rock samples. The experimental results of two rock types, namely

Bohus granite and Ekberg marble, are used in this work. The Bohus granite was medium grained (mean size around 1.8 mm) with maximum grain sizes of potassium feldspar of up to 1 cm and quartz up to 3.6 mm. The Ekberg marble was fine- to medium-grained with an average grain size of 0.27 mm. All the rock samples were taken carefully from the field where the rocks were quite isotropic. Some physical and mechanical property data of the rocks are given in Table I.

Rock samples, 100 mm in length and 116 mm in diameter, were cast in steel tubes and cemented in place. A hemispherical indenter of diameter 13.2 mm was used with quasi static loads ranging from 10 to 100 kN.

After indentation tests, the rock samples were gently pressed out of the tubes and sectioned into two to five slabs about 3 mm thick (Figure 1). Both sides of a slab were treated with fluorescence penetrant for crack discrimination. The main post-test procedures were as follows: clean the slab surfaces; apply the penetrant; clean away the remaining penetrant on the surface and spray a thin layer of developer. The surfaces were then ready for observation in ultraviolet light. Photos were taken both in ultraviolet light and nature light. Typical views of the granite and marble samples are shown in Figures 2 and 3 respectively, which are the first two neighbouring views taken at the centre section of the sample. A multitude of cracks were observed at different load levels.[19] The cracks were seen more clearly in the granite than in the marble. The bright areas in the photos of marble (Figure 3) resulted from the permeation of fluorescence penetrant into the micro cracks and the boundaries of the fine-grained rock. A side crack stretched out to the side (Figure 3), which is another type of indentation crack not generated by the splitting mechanism. The subsurface cracks propagated radially with increase in load and formed a fan pattern at high levels of load.

Splitting fracture model

The splitting fracture model[16] deals with the crack propagation in the direction of compression and explains very well the non-linear deformation and failure of brittle rocks caused by

Table I. Rock parameters

Rock parameters	Bohus granite	Ekeberg marble
Density, ρ (kg/m^3)	2634	2848
Uniaxial compressive strength, σ_c (MPa)	152.8	160.4
Young's modules, E (GPa)	64.1	84.4
Poisson's ratio, v	0.31	0.35
Fracture toughness (MPa m$^{1/2}$)	2.7	2.0

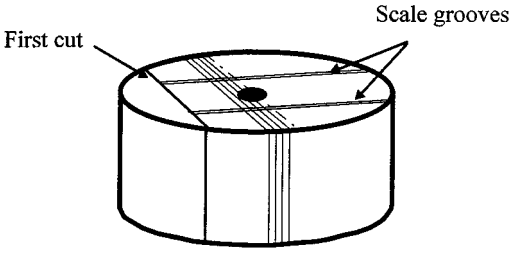

Figure 1. Sectioning of rock samples

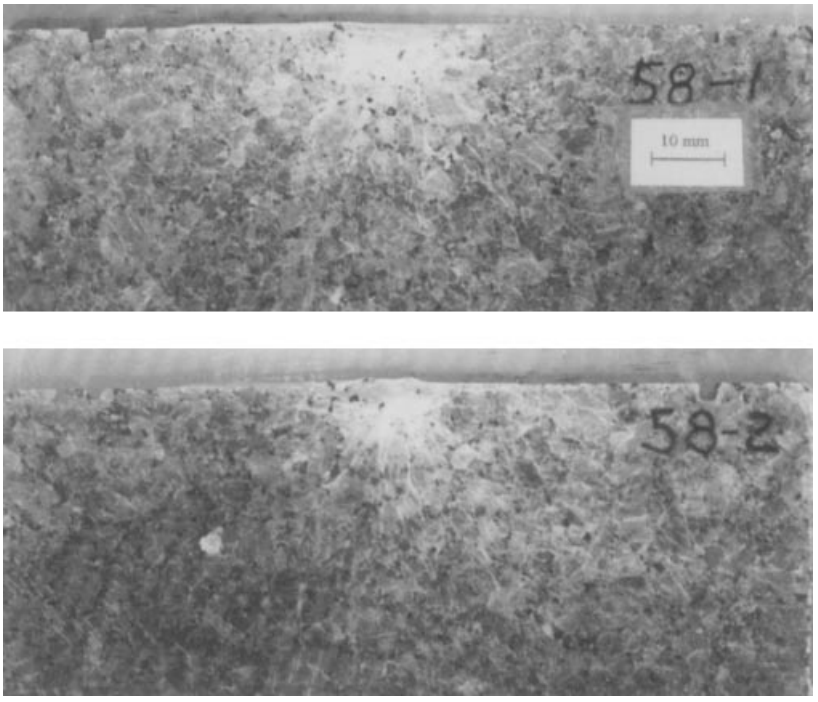

Figure 2. Photos of granite taken in nature light (Load = 102 kN, after Reference 19)

compression. The detailed derivations of the model can be seen in References 16 and 17. In the fracture model, it is assumed that many original micro cracks exist in the rocks. The splitting cracks or wing cracks are initiated at the tips of these pre-existing cracks. In compression, the shear (mode II) cracks will initiate when the stress intensity factor K_{II} at the crack tips exceeds the critical K_{IIC}, that is

$$K_{IIC} = \tau_{eff}(\pi a_0)^{1/2} \tag{1}$$

and the effective shear stress τ_{eff} is given by

$$\tau_{eff} = \tau - \tau_f = \tau - \sigma_n \tan \phi \tag{2}$$

where a_0 is half of the original crack length, ϕ is friction angle, τ, τ_f are internal shear and frictional stresses on the surface of the original crack respectively, σ_n is normal stress on the surface of the original crack, and τ and σ_n are functions of the major principal stresses according to the Mohr circle diagram. Substituting the Mohr stress functions into equation (2) we gain the effective shear stress

$$\tau_{eff} = \sigma_1 \cos\theta(\sin\theta - \cos\theta \tan\phi) - \sigma_2 \sin\theta(\cos\theta - \sin\theta \tan\phi) \tag{3}$$

where σ_1, σ_2 are the two principal stresses and θ is the direction of the original crack surface. Here compression is defined as positive.

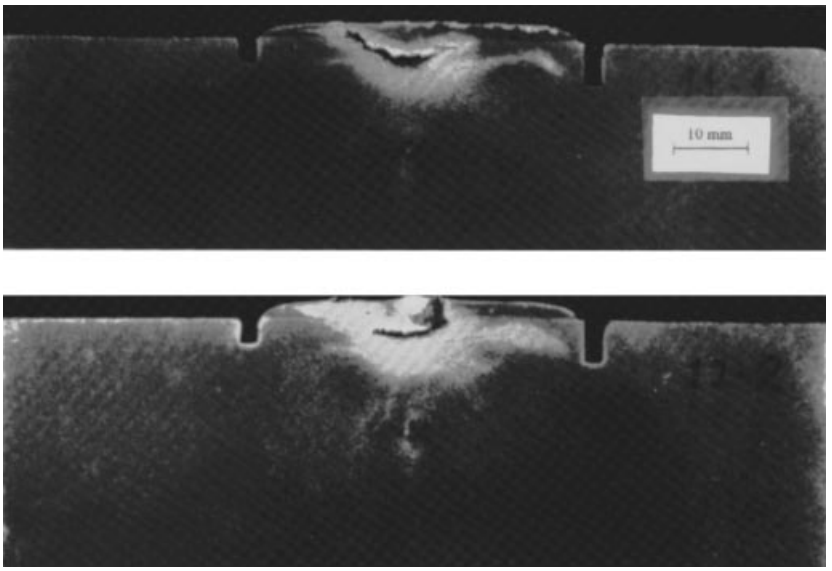

Figure 3. Photos of marble taken in ultraviolet light (Load = 38.9 kN, after Reference 19)

The configurations of the stresses and cracks are illustrated in Figure 4. Substituting equation (3) into equation (1), the critical stress for the initiation of wing cracks are obtained.

The wing crack extends and turns gradually in the direction of the major principal compressive stress (Figure 4(a)). The fracture process shown in Figure 4(a) is transformed into the case in Figure 4(b) for mathematical simplicity. It can then be treated as a tensile fracture driven by an equivalent wedge force F on the crack surface. F is obtained from the resultant shear and normal force components imposed on the initial crack surface. It is expressed as

$$F = 2a_0[\sigma_{n'} \sin\theta - \tau_f \cos\theta] = a_0[(\sigma_1 - \sigma_2) f(\theta, \phi) - 2\sigma_2 \cos\theta \tan\phi] \tag{4}$$

where $f(\theta, \phi) = (1 + \cos 2\theta)(\sin\theta - \cos\theta \tan\phi)$, $\sigma_{n'} = \sigma_n - \sigma_2$, effective normal stress.

Here σ_2 is subtracted from σ_n in calculating the effective normal force, because the rock can be considered as subjected to the hydraulic pressure σ_2 and the differential stress $(\sigma_1 - \sigma_2)$ acting along the direction of σ_1. The hydraulic pressure σ_2 does not induce any wing cracks, but it induces certain friction resistance on the crack surface. The differential stress $(\sigma_1 - \sigma_2)$ is the driving 'force' for the formation of wing cracks.

For the crack subjected to the wedge force F and the lateral stress σ_2 (Figure 4(b)), the stress intensity factor K_I is given by

$$K_I = \frac{F}{\sqrt{(\pi L)}} - \sigma_2 \sqrt{(\pi L)} \tag{5}$$

With the growth of the wing crack, the stress intensity factor will be K_{IC}. Transforming equation (5) yields the length of the wing crack as

$$L_P = \frac{1}{4\pi}\left[\frac{\sqrt{(K_{IC}^2 + 4F\sigma_2)} - K_{IC}}{\sigma_2}\right]^2 \tag{6}$$

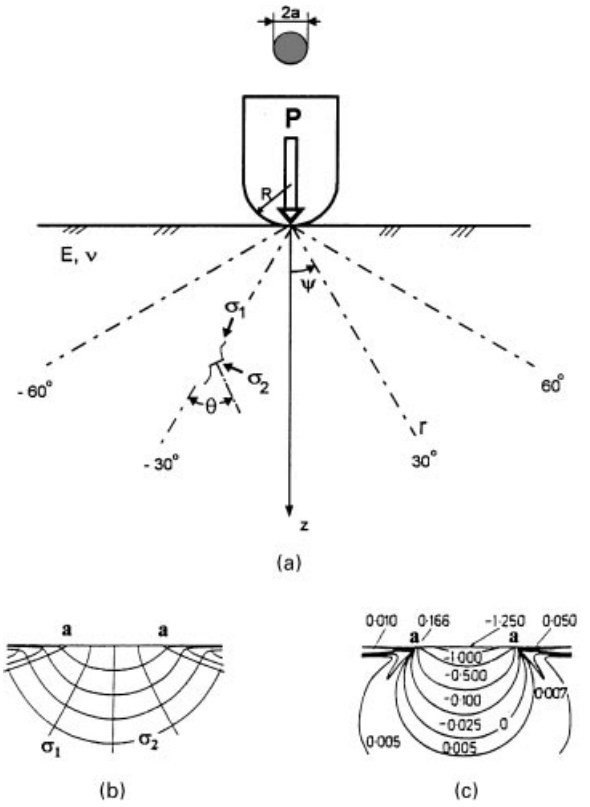

Figure 4. (a) Indentation co-ordinates (b) two principal stress trajectories, and (c) counter of minor principal stress (σ_2) in the axially symmetrically plane. (Note: the diagrams (b) and (c) are taken from Reference 20 with our variable conventions. The numbers in (c) are the ratio of σ_2 to the average load pressure ($P/\pi a^2$), where the minus sign indicates compression.)

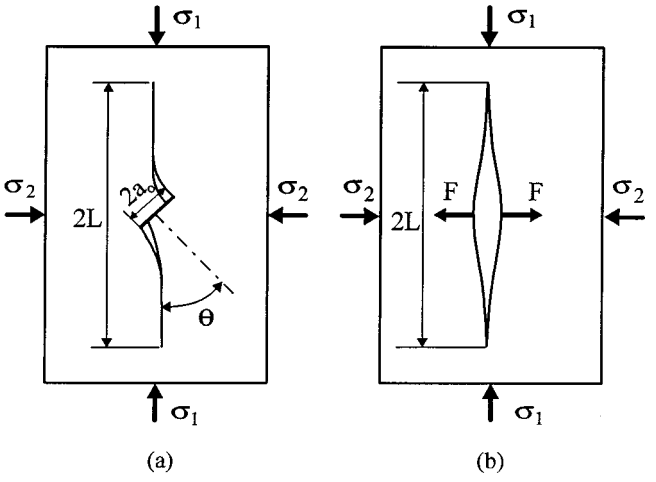

Figure 5. Development of a wing crack (after Reference 16)

where L_P is the apparent growth of the wing crack and K_{IC} is the mode I fracture toughness.

The initial length of the apparent wing crack L_{P0} is obtained from equation (6) at critical stresses, while the initial physical length is defined as the projection of the original crack length along the σ_1 direction, that is, $L_0 = a_0 \sin\theta$. Here the physical length L and L_P are not identical. It is assumed in the model that the physical length of the wing crack, L, is proportional to L_P. Therefore, we obtain the wing crack length:

$$L = L_P \frac{L_0}{L_{P0}} \tag{7}$$

Simulation of subsurface fracture

The Hertizian stress field induced by two elastic balls of radii R_1 and R_2 in contact[20] is used for describing the stresses caused by a hemispherical indenter, in which the indenter is assumed to be rigid and the rock semi-infinite. The major principal compressive stress σ_1 follows the trajectories shown in Figure 4(b). The magnitudes of σ_1 are many times larger than those of σ_2 outside the compressive zone (see the zero contour in Figure 4(c)). Therefore the indentation field is dominated by compression. Application of the splitting fracture model to the simulation of the indentation subsurface would be appropriate.

Considering that the stresses are axi-symmetrical, the subsurface fracture are assumed to develop in an axi-symmetrical plane. The principal stresses, σ_1 and σ_2, in the axi-symmetrical plane are considered. The original cracks are characterized by four parameters, ψ, r, θ and a_0 (depicted in Figures 4 and 5). Original cracks with their centre located along three radial lines of angles $\psi = 0^\circ$, 30° and 60° respectively and at distances a few times that of the contact radius, i.e. $r/a = 0, 1, 2, 3$ respectively from the origin (see Figure 4) are investigated. The critical loads for the initiation of wing cracks are calculated by equations (1)–(3). The propagation of wing cracks is calculated by equations (4)–(7). The magnitude of the frictional angle ϕ is 30° for the two rock types.[23] The original micro cracks in the direction with maximum τ_{eff} are the easiest to initiate. In our simulation we consider only this weakest situation. The direction angle is given by $\theta = 45^\circ + \phi/2 = 60^\circ$.

The crack developments at the representative points in the field for a given load and initial crack length ($2a_0$) are illustrated in Figure 6. The crack lengths at different load levels are shown in Figure 7. It is seen that on the centre line ($\psi = 0^\circ$) crack development near the indenter ($r/a = 1$) is much constrained. Close to the indentation centre where all the principal stresses are compressive and of similar magnitude, no crack initiation occurs. At some distance away,

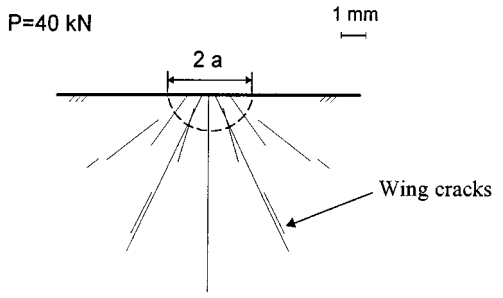

Figure 6. Fracture pattern of the representative cracks

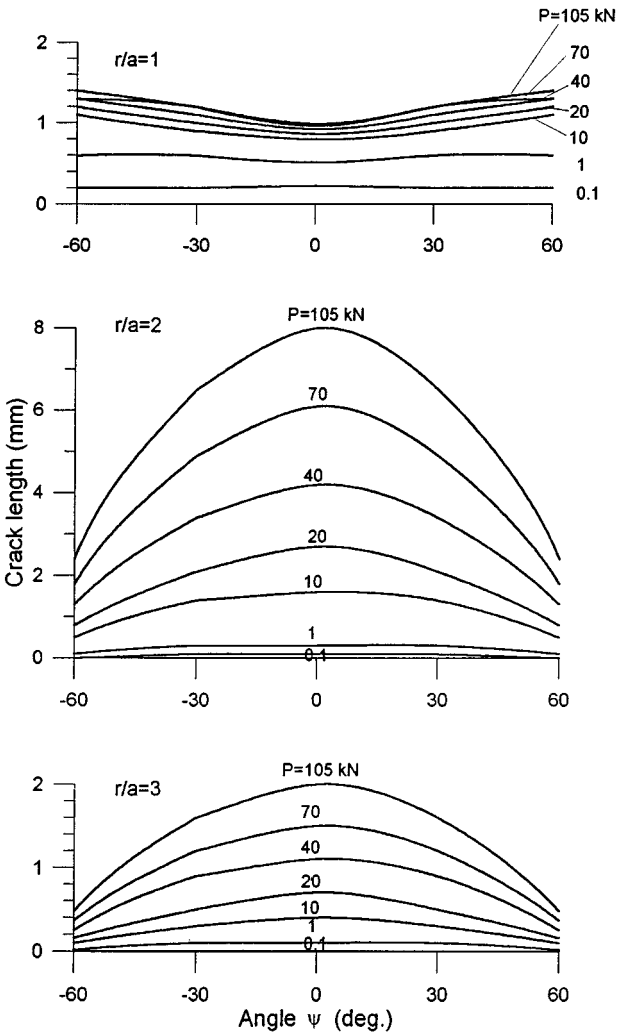

Figure 7. Fracture development at different distances from the indenting centre

maximum crack development is achieved. This is more distinct along the z axis ($\psi = 0$) than along side directions (Figure 8). The larger the magnitudes of σ_1 and $(\sigma_1 - \sigma_2)$, the longer the fractures. Hence a fan patterned crack front is created (Figure 6). The values of σ_1 and σ_2 are in proportion to the indentation load P, and different critical loads are needed to drive the cracks at different locations. The long cracks at the middle may intersect with the cracks further away which are along the same radial paths. This overlapping of the cracks generates long cracks, such as the cracks along the z axis in Figure 6.

Comparison with experimental results

The calculated indentation subsurface fractures follow generally the trajectories of the major principal compressive stress σ_1 (Figure 4(b)) and form a fan pattern of distribution (Figure 6), which is similar to those observed in Figures 2 and 3.

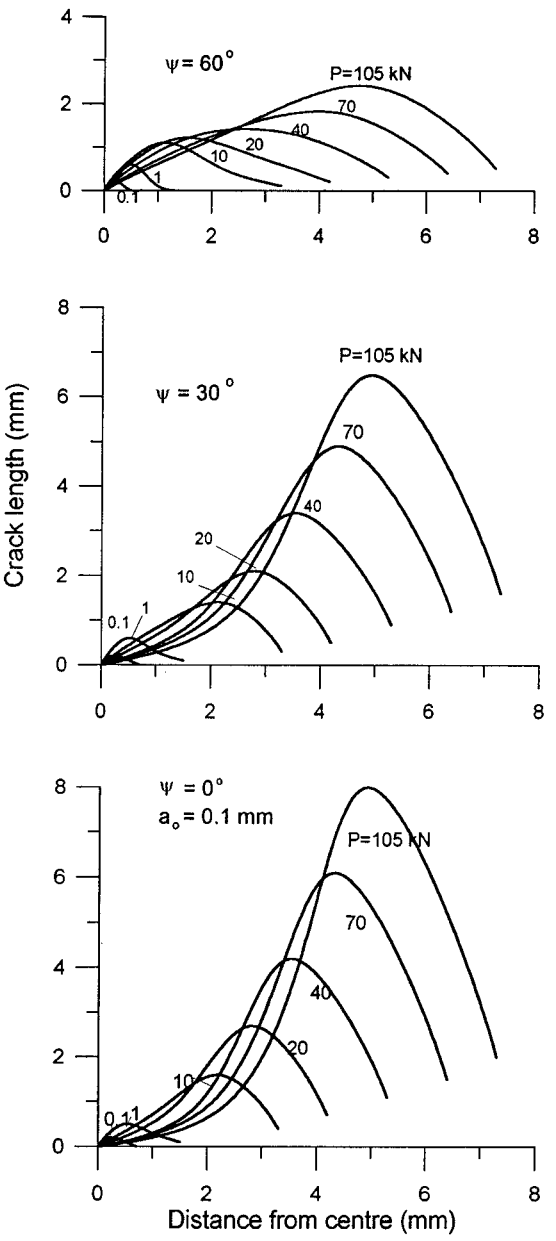

Figure 8. Fracture development along radial directions

The depth of the subsurface fractures (in the z direction) is simulated and the results compared with the measurements from the indentation experiments. The depth is measured from the lower tip of the fracture originated at $r/a = 2$ to the rock surface, where the fracture has the largest depth. The simulation parameter $2a_0$ is varied to find the depth coincident with the experiments. For granite it ranges from 300 to 400 μm, and for marble from 200 to 240 μm. The former is within the ranges observed by Sprunt and Brace[21] and Kranz[22] in the same kind of rock and the

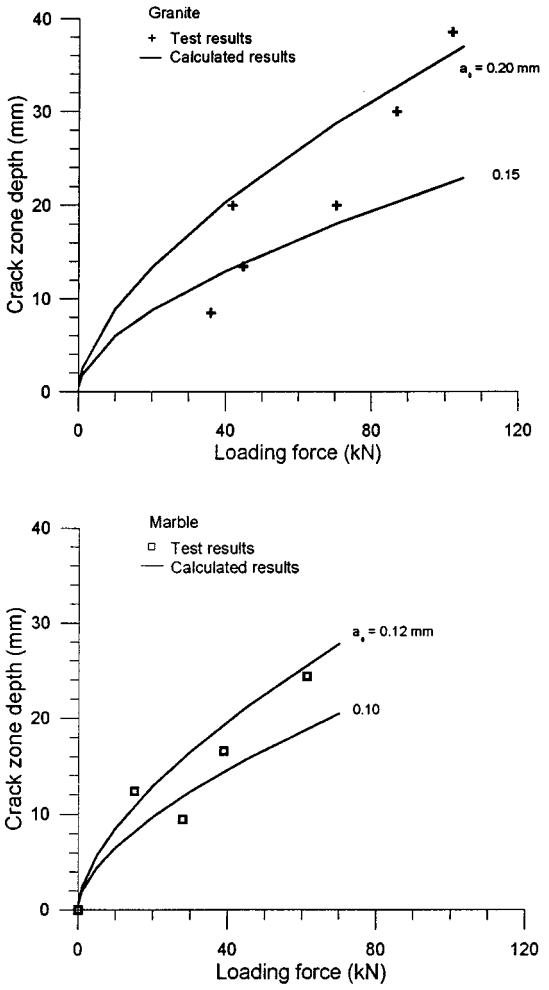

Figure 9. Simulation of fracture depth for granite and marble

latter is of the same order of magnitude as the rock grain size. The crack depth–load relationships are also in good agreement with the experiments of the two rocks (Figure 9).

DISCUSSIONS

The modelling of indentation fractures requires proper formulation of the indentation stresses and the fracture model. In this study, the elastic stress solution is applied for simplicity, which is valid in the area outside the crushed zone (roughly $r/a \geqslant 1$). This simplification is acceptable for the rocks undergoining small deformation and micro cracking.[16] The splitting fracture model describes fractures propagation along the trajectory of the major principal compressive stress in a compression dominated field. The rock indentation stress field has a similar feature. The fracture (see Figures 2 and 3) are driven mainly by compressive splitting, and the rock is buckled and split.[16,24]

In the non-uniform indentation stress field, the fracture resistance at the two crack tips is not identical. Due to the large confinement stress (σ_2) near the indenting centre, the upper wing may be under-developed and the lower wing over-developed. For simplicity, we consider only the stresses at the middle point of the original crack. This may cause the positions of the predicted cracks to the nearer to the indenter than in practice. The non-uniform effect is trivial at the initial stage when the cracks are very short and the stress difference is negligible. The unsymmetrical development of the wing crack might be accounted for by shifting the acting point of the wedge force from the middle according to the extent of unsymmetry. The two crack tips will not extened simultaneously. A bias of the splitting force will thus be incurred, and it varies also with fracture propagation. This will entail much complicated calculations.

The simulation lengths of the original cracks in granite are in the range of 200–400 μm, which are within the range of magnitudes as those observed by Sprunt and Brace[21] and Kranz.[22] They have shown that for the coarse-grained granite the length of original cracks is distributed among ten to one thousand μm with an average value of about 100 μm. Our simulated original crack lengths are a few times larger than the average value. The lengths for the marble are relatively large, close to the average rock grain size. This is attributed to the fact that large micro cracks are close or of the same order of magnitudes as the grain size and will dominate in the fracture initiation and propagation. Meanwhile the smaller cracks are inhibited once the larger cracks start growing.[15] Therefore, larger cracks play a major role in the fracture process.

The determination of fracture parameters in the model is also important in order to predict fracture development. The value of K_{IC} (1 MPa $m^{1/2}$) for granite in our modelling is smaller than that measured in the laboratory (see Table I). It is determined through simulation of the rock stress–strain behaviours obtained both from the uniaxial and biaxial tests.[16] Similarly a smaller value of 0.7 MPa $m^{1/2}$ of K_{IC} is used for the marble. The employment of smaller K_{IC} values is because the cracks we are dealing with are micro cracks. The process zone in front of the crack tip is much smaller than that of macro cracks, so the fracture resistance is smaller.[16,24] The fracture toughness used here represents the average resistance to fracture for the small scaled cracks of our concern.

In the model simulation, only the weakest original cracks in the direction with maximum effective shear stress on the crack surfaces are considered. Cracks oriented in other directions or with different lengths can also be calculated in a similar way, which will lead to larger critical loads and shorter crack developments. The extreme crack orientation is at $\theta = 0^\circ$. The crack is closed and no fracture can every occur. The minimum θ for wing crack initiation can be obtained from equations (1)–(3).

For simplicity, the crack model does not consider crack interaction, except for the overlapping cracks. Eventually fracture interaction will cause fracture development in some specific directions and inhibit others.[15,24] The model application can be considered as an indication of the average situation.

In the splitting model, the wedge force disappears if the sliding faces of the original crack lose contact. This will give rise to an unstable cracking. This might happen when the lateral tensile stress is large enough to cause open cracks or a large deformation in compression results. In the Hertzian stress field, the lateral tensile stress σ_2 is very small, only about 1/50 of σ_1. The deformation in the rock body is not significant. The observations of the indentation process and crack photos revealed that unstable radial cracks were rarely found in these two kinds of rocks.

So far, we have considered only the indenter-induced stresses. The hemispherical indenter produces larger differences in the principal stresses than an indenter with uniform loading pressure.[25] In rock fragmentation, therefore, a hemispherical indenter is preferred to a flat or truncated indenter.

The splitting fracture model is two dimensional. In reality, fractures are formed in a three-dimensional condition. Experiments on 3-D disc-like crack in glass and PMMA (polymethylmethacrylate)[18] showed that the additional 3-D constraint hindered the propagation of 3-D wing cracks, and that no significant growth could occur for a single 3-D crack. Nevertheless, the interaction and coalescence of a multitude of cracks make the 3-D crack development similar to the 2-D form.[18] This may be justified by the satisfactory simulation of the rock behaviour by the 2-D constitutive models.[17,18]

The splitting fracture model has been applied in modelling crack propagation in an indentation stress field. Moreover, it is applicable to other stress situations with the same fracture mechanism, for example, the instability of a rock pillar and borehole breakout.[26]

CONCLUSIONS

The simulation results of rock indentation subsurface fractures are in good agreement with the indentation experiments. The subsurface fractures are driven by the shear-splitting mechanism and form a fan pattern.

Factors influencing the fracture propagation are the indentation stress state and fracture properties of rock. The stress state is dependent upon the total load, indenter shape, indenter size and rock properties. The larger the principal stress, σ_1, and the differential stress, $(\sigma_1 - \sigma_2)$, the longer the splitting fractures.

ACKNOWLEDGEMENTS

The authors would like to thank the Swedish Nuclear Fuel and Waste Management Company (SKB) for its financial support (project no. 16450140). The petrograhic descriptions made by Berit Alm are appreciated. Acknowledgement is made to Dr. Chunlin Li for constructive discussions concerning the fracture model and its application.

REFERENCES

1. H. Wagner and E. R. H. Schümann, 'The stamp-load bearing strength of rock — an experimental and theoretical investigation', *Rock Mech*, **3/4,** 185–207 (1971).
2. M. Hood, 'Phenomena relating to the failure of hard rock adjacement to an indentor', *J. South African Inst. Min. Metallurgy*, Dec., 113–123 (1977).
3. G. E. Korbin, 'Fractors influencing the performance of full face hard rock tunnel boring machines', *Technical Report UMTA-CA*-06-0122-79-1 (for Urban Mass Transportation Administration), Washington, DC 1979.
4. N. G. W. Cook, M. Hood and F. Tsai, 'Observation of crack growth in hard rock by an indenter', *Int. J. Rock Mech. Min. Sci. Geomech. Abstr.*, **21**(2)**,** 97–107 (1984).
5. A. Kumano and W. Goldsmith, 'An analytical and experimental investigation of the effect of impact on coarse granular rocks', *Rock Mech.*, **15,** 67–97 (1982).
6. P.-A. Lindqvist, H. H. Lai and O. Alm, 'Indentation fracture development in rock continuously observed with a scanning electron microscope', *Int. J. Rock Mech. Min. Sci. Geomech. Abstr.*, **21** (4)**,** 165–182 (1984).
7. D. L. Sikarskie and N. J. Altiero, 'The formation of chips in the penetration of elastic–brittle materials', *J. Appl. Mech.*, **40**(3)**,** 791–798 (1973).
8. S. S. Pang and W. Goldsmith, 'Technical note: investigation of crack formation during loading of brittle rock', *Rock Mech. Rock Eng.*, **23,** 53–63 (1990).
9. B. Lundberg, 'Penetration of rock by conical indenters', *Int. J. Rock Mech. Min. Sci. Geomech. Abstr.*, **11,** 209–214 (1974).
10. D. H. Zeuch, D. V. Swenson and J. T. Finger, 'Subsurface damage development in rock during drag-bit cutting: observations and model predictions', *24th U.S. Symp. on rock Mech.,* 1983, pp. 733–742.
11. S. S. Pang, W. Goldsmith and M. Hood, 'A force-indentation model for brittle rocks', *Rock Mech. Rock Eng.*, **22,** 127–148 (1989).
12. G. Wijk, 'The stamp test for rock drillability classification', *Int. J. Rock Mech. Min. Sci Geomech. Abstr.*, **26**(1)**,** 37–44 (1989).

13. B. N. Whittaker, R. N. Singh and G. Sun, *Rock Fract. Mech — Principles, Design and Applications*, Elsevier, Amsterdam, 1992.
14. G. Sun, B. N. Whittaker, R. N. Singh and M. D. Waller, 'Prediction of rock cutting performance using fracture mechanics principles — a review' *Proc. 11th Int. Conf. on Ground Control in Mining*, Wollongong, Australia, 7–10 July 1992.
15. H. Horii and S. Nemat-Nasser, 'Compression-induced microcrack growth in brittle solids: axial splitting and shear failure', *J. geophys. Res.*, **90,** 3105–3125 (1985).
16. C. Li and E. Nordlund, 'Deformation of brittle rocks under compression — with particular reference to micro cracks', *Mech. Matter.*, **15,** 223–239 (1993).
17. C Li, 'Micromechanics modelling for stress–strain behaviour of brittle rocks', *Int. j. numer anal. methods geomech.*, **19,** 331–344 (1995).
18. L. N. Germanovich, R. L. Salganik, A. V. Dyskin and K. K. Lee, 'Mechanics of brittle fracture with pre-existing cracks in compression', *Pageoph*, **143,** 117–149 (1994).
19. P.-A. Lindqvist, L. M. Suarez, M. Montoto, X. C. Tan and S. Q. Kou, 'Rock indentation data base — testing procedure, results and main conclusions', *SKB* (Swedish Nuclear Fuel and Waste Management Co.) *Project Report PR 44-94-023,* 1994.
20. B. Lawn and R. Wilshaw, 'Review indenation fracture; principles and applications', *J. Mater. Sci.*, **10,** 1049–1081 (1975).
21. E. S. Sprunt and W. F. Brace, 'Direct observation of microcavities in crystalline rocks', *Int. J. Rock Mech. Min. Sci. Geomech. Abstr.* **11,** 139–150 (1974).
22. R. L. Kranz, 'Micro-cracks in rock', *Tectophysics*, **100,** 449–480 (19083).
23. J. C. Jaeger and N. G. W. Cook, *Fundamentals of Rock Mechanics*, Chapman and Hall, London, 1979.
24. Z. P. Bazant and L. Cedolin, *Stability of Structures — Elastic, Inelastic, and Damage Theories*, Oxford University Press, London, 1991.
25. K. L. Johnson, *Contact Mechanics*, Cambridge University Press, Cambridge, 1985.
26. L. N. Germanovich, J.-C. Roegiers and A. V. Dyskin, 'A model for borehole breakouts in brittle rocks', *Rock Mech. Petrol. Eng. Eurock '94*, Balkema, Rotterdam, 1994, pp. 361–370.